Development of a gamma-ray imager using a large area monolithic 4 × 4 MPPC array for a future PET scanner

2012 JINST 7 C01083

(http://iopscience.iop.org/1748-0221/7/01/C01083)

PUBLISHED BY IOP PUBLISHING FOR SISSA

RECEIVED: *November 4, 2011*
REVISED: *December 20, 2011*
ACCEPTED: *January 4, 2012*
PUBLISHED: *January 24, 2012*

THE 9th INTERNATIONAL CONFERENCE ON POSITION SENSITIVE DETECTORS,
12–16 SEPTEMBER 2011,
ABERYSTWYTH, U.K.

Development of a gamma-ray imager using a large area monolithic 4×4 MPPC array for a future PET scanner

T. Nakamori,[a,1] **T. Kato,**[a] **J. Kataoka,**[a] **T. Miura,**[a] **H. Matsuda,**[a] **K. Sato,**[b] **Y. Ishikawa,**[b] **K. Yamamura,**[b] **N. Kawabata,**[b] **H. Ikeda,**[c] **G. Sato**[c] **and K. Kamada**[d]

[a] *Research Institute for Science and Engineering, Waseda University, 3-4-1, Ohkubo, Shinjuku, Tokyo, Japan*
[b] *Solid State Division, Hamamatsu Photonics K.K., 1126-1, Ichino-cho, Hamamatsu, Shizuoka, Japan*
[c] *ISAS/JAXA, Yoshinodai, Chuo-ku, Sagamihara-shi, Kanagawa, Japan*
[d] *Materials Research Laboratory, Furukawa Co., Ltd., 1-25-13, Kannondai, Tsukuba, Ibaraki, 305-0856, Japan*

E-mail: nakamori@aoni.waseda.jp

ABSTRACT: We report the development of a monolithic MPPC array, which consists of $3\times3\,mm^2$ elements arranged as a 4×4 array manufactured by Hamamatsu applicable to next generation PET scanners. We show that the MPPC is suitable for time of flight PET applications by simple measurement using coincident back-to-back 511 keV gamma rays. We demonstrated that the MPPC has much better timing resolution of ~ 600 ps than the APD. We coupled the monolithic MPPC array with the Ce:LYSO and Pr:LuAG scintillator matrices as gamma-ray detectors. The energy resolutions were evaluated as $\sim 14\%$ with 662 keV gamma-rays and the Ce:LYSO achieved the best. We also used a resistor network readout circuit with some optimization. The averaged positional resolution is estimated as ~ 0.27 mm in both x and y directions, while the energy resolution of each pixel was 9.9% for 662 keV gamma rays. Finally we applied the GHz class fast sampling waveform acquisition system to improve performance, and demonstrated efficient noise reduction by the clear detection of 22 keV gamma rays.

KEYWORDS: Gamma camera, SPECT, PET PET/CT, coronary CT angiography (CTA); Medical-image reconstruction methods and algorithms, computer-aided so

[1] Corresponding author.

doi:10.1088/1748-0221/7/01/C01083

2012 JINST 7 C01083

Contents

1 Introduction **1**

2 Comparison of the time of flight resolution **2**

3 Performances of the MPPC array and the scintillator matrices **4**
3.1 4×4 MPPC array 4
3.2 Performances with pixelized scintillators 5

4 Charge division readout **6**

5 Waveform acquisition **8**

6 Discussion and conclusion **11**

1 Introduction

Positron emission tomography (PET) is a well-established functional imaging method for detection and diagnosis of cancers and Alzheimer's in their early stages [1]. Currently, the PET combined with computed tomography (CT) has become more common as a multimodality imaging device [2], as it provides an improved insight into the spatial and temporal interrelations between functional and anatomical images. The CT imaging suffers from poor soft-tissue contrast with patients also subjected to a significant radiation dose that exceeds that received from the PET itself, while Magnetic Resonance Imaging (MRI) offers excellent soft-tissue contrast and anatomical detail without the additional radiation. Many advantageous aspects of MRI-PET are now being proposed and testing of their prototypes is underway e.g., [3], though there are several problems to be solved. A Photo-Multiplier Tube (PMT) incorporated in conventional PET scanners does not work within the MRI high Magnetic field, and the spatial resolution attainable with a PMT-based PET is far from the theoretical limit of PET resolution due to its bulky volume. Recently various PET modules utilizing an avalanche photodiode (APD) which is a compact semiconductor photo-detector have successfully demonstrated the potential for simultaneous MRI-PET imaging [4] as well as ultimate sub-millimeter spatial resolutions [5], even though the APDs are easily affected by electric noise due to the relatively low avalanche gain (typically ~ 100).

Multi-Pixel Photon Counter (MPPC), also known as a Silicon Photo-Multiplier (SiPM), has been eventually developed as a compact, high performance semiconductor photodetector consisting of multiple minute Geiger-mode APD pixels arranged as a 2-dimensional array. Its operating principles and basic performance are introduced in [6]. The MPPC has many advantages like APDs, such as insensitivity to magnetic fields, effective time resolution and compactness. In addition, it is operated in Geiger-mode, meaning its gain may be almost comparable to that of PMTs at up to the

2012 JINST 7 C01083

10^{5-6} level. Despite its superior advantages, however, it also has several weak points compared to traditional PMTs and APDs. For instance, the dynamic range of the MPPC is limited by the number of Geiger-mode APD pixels comprised in the device. Each of the latter is subject to dead time (typically measured in tens of ns) once the Geiger-discharge has triggered, during which multiple photons entering a single pixel cannot be counted, resulting in a non-linear response to the number of incident photons. Another problem is that thermal electrons also trigger a Geiger-discharge, resulting in substantial contamination of dark counts, typically amounting to 3 Mcps for $3\times3\,mm^2$ MPPCs (whose Geiger-mode APDs are arranged with a pitch of 50 mm) measured at $+25^{\circ}C$ [7]. Nevertheless, its great advantages make MPPC one of the ideal photo-sensors for MRI-PET and also for Time Of Flight (ToF) applications e.g., [8].

There is also a wide-ranging choice of scintillators to be used in the PET scanner. The most popular scintillator at present is Ce-doped $Lu_2(SiO_4)O$ (Ce:LSO) or Ce-doped $(Lu,Y)_2(SiO_4)O$ (Ce:LYSO) [9], both of which feature high light yield (75% of Tl:NaI), short scintillation decay time (40 ns) and high density ($7.4\,g/cm^3$) greater than BGO ($7.1\,g/cm^3$). Alternatively, brand-new scintillators with high light output and/or fast timing properties are being tested, especially for future applications in ToF-PET scanners. Pr-doped $Lu_3Al_5O_{12}$ (Pr:LuAG) is one such scintillator characterized by a very fast decay time (20 ns) and good light yield (53% of Tl:NaI) [10, 11]. Since standard APDs have poor quantum efficiency at its sharp spectral peak around 310 nm, dedicated UV-enhanced APD arrays have been specifically developed to readout the Pr:LuAG scintillators [12].

Currently, the development of a high-resolution MRI-PET/ToF-PET technique utilizing the newly designed MPPC array is underway. We have developed a large-area, monolithic 4×4 MPPC array and reported its performance as a gamma-ray detector coupled with Ce:LYSO and Pr:LuAG matrices [13] and this paper. The advantage of using MPPC monolithic arrays, instead of single MPPC devices assembled together [14], is that we can easily achieve good uniformity over the pixels of gain, PDE and dark counts. Moreover, the gap between each pixel can be minimized, thereby improving the effective area of the MPPC arrays as a whole.

This paper is organized as follows. In section 2, we present a comparison of timing resolution between APDs and MPPCs in order to prove that MPPCs are relatively suitable for ToF application. In section 3, we present the basic characteristics of a large-area monolithic 4×4 MPPC array developed. Subsequently we combined the MPPC array with various pixelized scintillator arrays as a probe of the compact gamma-ray imager, and tested the spectroscopic performance of the stacked detectors. In section 4, we applied a resistor network readout circuit to reduce the number of readouts and demonstrated successful event reconstructions of incident positions and energies for gamma rays. In section 5, in order to improve the energy resolution and lower the energy threshold, we employed a data acquisition system with a fast wave form digitizer chip. The initial spectroscopic performance is presented using a single element MPPC. Finally the conclusions are presented in section 6.

2 Comparison of the time of flight resolution

Time of flight (ToF) information between back-to-back gamma rays can constrain the location of the 511 keV gamma rays meaning an improved signal-to-noise ratio could be expected in obtained

2012 JINST 7 C01083

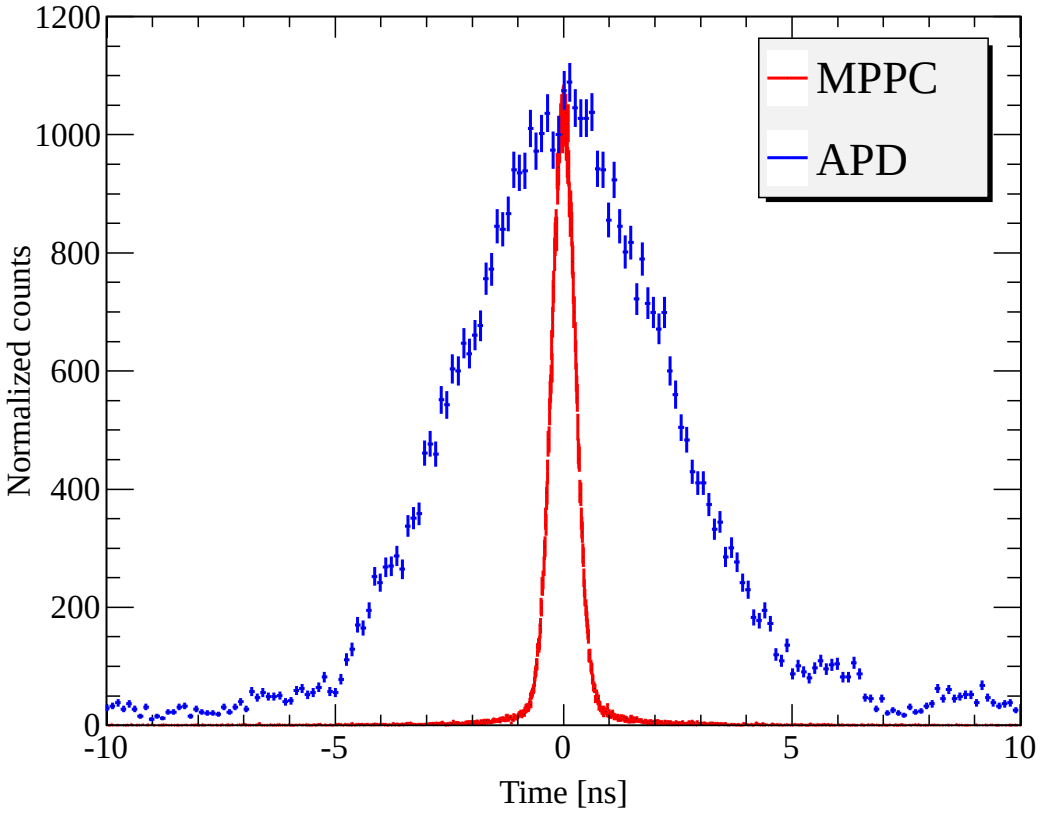

Figure 1. Timing spectra measured with the annihilation quanta from a ^{22}Na source. The broader and thinner distribution is derived from measurement with APDs and MPPCs, respectively.

images. Semiconductor devices could be potential alternatives to current ToF-PET scanners using PMTs. In this section we present a comparison between APDs and MPPCs for timing resolutions using back-to-back 511 keV gamma rays at 20°C. Two pairs of APDs and MPPCs are prepared both of which are optically coupled with a $3\times3\times10\,\mathrm{mm}^3$ Ce:LYSO scintillator using silicone optical grease (OKEN 6262A). The APDs used were the S8664 series (Hamamatsu) with the $3\times3\,\mathrm{mm}^2$ type operated at a gain of 50, while the MPPCs were single channel models S10362-33-050C (Hamamatsu), consisting of 3600 Geiger-mode APDs of 50 μm pixels. The operated gain of the MPPC here was 9×10^5. A ^{22}Na source was placed in the middle between the two scintillator elements. Each of the signals from the APDs was fed into charge sensitive amplifiers (Clear Pulse CP580), while the those from the MPPCs were not connected to any amplifies. One of the signals, through a constant fraction discriminator, triggered a time to analog converter (TAC) while the other with fixed delay, was used for the stop signal to the TAC. Figure 1 shows the timing spectra obtained for the APDs and MPPCs. It is apparent that the MPPC has better timing resolution by almost a factor of 10, where the FWHMs are 5300 and 634 ps for the APD and MPPC, respectively. The APD itself has a nice timing resolution of wellunder 1 ns, which is confirmed by a synchrotron X-ray beam experiment [5]. Due to the moderate gain of 50–100, however, the APDs always

2012 JINST 7 C01083

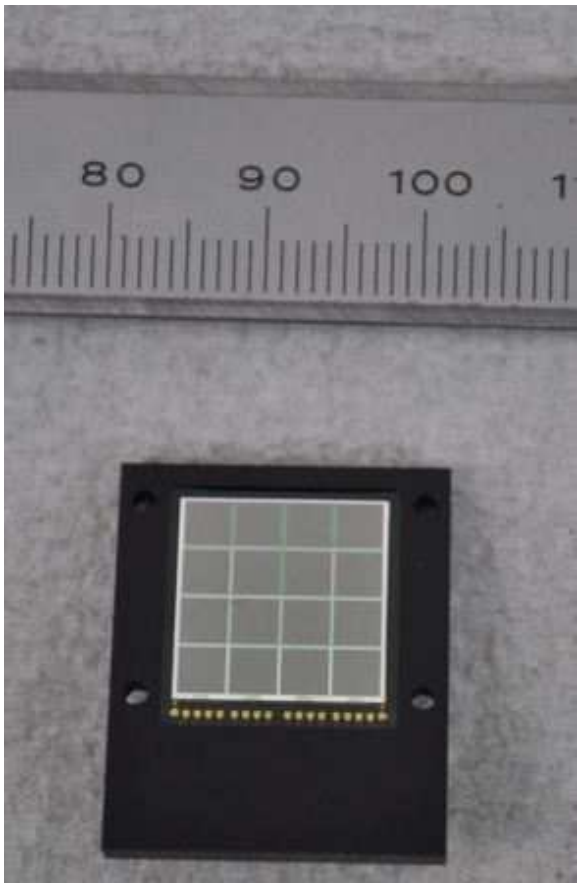

Figure 2. A picture of the MPPC array.

require charge sensitive amplifiers that critically limit the timing resolution, when the APD is used as a scintillation detector. Conversely, the MPPC can work without amplifiers (or sometimes with a fast current amplifier) since its high gain generates numerous charges. Therefore the development of an MPPC-based PET detector is highly motivated in order to accomplish advanced ToF-PET scanners with semiconductor photo-sensors.

3 Performances of the MPPC array and the scintillator matrices

3.1 4×4 MPPC array

The large-area monolithic MPPC array described here was specifically designed and developed for future applications in nuclear medicine (e.g., PET scanners) by Hamamatsu Photonics K.K. The MPPC array consists of a 4×4 array of individual $3\times3\,mm^2$ pixels and a 0.2 mm gap between them. Each pixel comprises 60×60 Geiger-mode APDs arranged with a pitch of 50 mm. The MPPC array tested here is placed on a printed wiring board (PWB) package 25.0 by $21.0\,mm^2$ and 2.7 mm thick, and using conventional epoxy resin as an entrance window (figure 2). All 4×4 pixels have a common cathode through which the positive bias voltage is supplied, whilst signals from individual anodes can be read through the signal pins gathered at the bottom-side of the PWB. The

2012 JINST 7 C01083

Table 1. Specification of the MPPC array at 25°C

Parameters	Numbers
Number of elements	16 (4×4)
Active area/channel (mm^2)	3×3
Size of a Geiger mode APD (μm^2)	50×50
Typical photon detection efficiency (%)	50
Terminal capacitance/channel (pF)	320
Operation voltage (V)	73.0±0.12
Gain	7.5×10^5
Typical dark current/channel (μA)	3

Table 2. Characteristics of the scintillators

	Ce:LYSO	Pr:LuAG
Density (g cm^{-3})	7.10	6.73
Light yield (photon/MeV)	2.5×10^4	2.0×10^4
Decay time (ns)	40	20
Peak wavelength (ns)	420	310

dark count of each MPPC pixel ($3 \times 3\,mm^2$) is typically 2 MHz at the 1 p.e. level threshold with a gain of 7.5×10^5 measured at 0°C. This amount of the dark count is relatively large, since the array we tested was produced in early stages. We've already confirmed the dark count is suppressed as low as $\sim$ 400 kHz even at 20°C in the latest products. Hereafter all the measurements in this paper were conducted at 0°C to reduce the contamination of dark counts. Other basic characteristics of the MPPC array are summarized in table 1.

The gain characteristic of each 4×4 MPPC pixel was measured as a function of bias voltage, using a weak blue light (465 nm) of a light emitting diode (LED). The charges generated by the MPPC were estimated from the single photoelectron peak channel which was individually taken with charge-sensitive ADC (HOSHIN V005; hereafter CSADC) after the amplification by a factor of 100. The result shows generally good linearity between 70.9 and 71.9 V, corresponding to the measured gain of $\sim$ 4–10 $\times 10^5$. The gain measured at a bias voltage of 71.9 V varies only ±7.2% over 4×4 MPPC pixels, where the average gain was 9.68×10^5. The array has turned out to have quite good uniformity. More details of the characteristic studies are described in [13].

3.2 Performances with pixelized scintillators

In our experiments, Ce:LYSO and Pr:LuAG were chosen to be coupled with the MPPC array described above. The basic parameters of Ce:LYSO and Pr:LuAG are summarized in table 2. The peak wavelength of Ce:LYSO favors MPPC because the latter is sensitive within the range 350–650 nm [6]. In this sense, a UV light emission of Pr:LuAG, peaking at 310 nm,is not favorable but its short decay time (20 ns) is particularly noteworthy as implemented in future ToF-PET scanners (see section 1) and also beneficial for MPPC to effectively reduce dark counts within a narrower coincidence window. We therefore fabricated another sample, Pr:LuAG(WLS), which was coated with a wavelength shifter layer of 20 μm that converts the 310 nm scintillation light of the Pr:LuAG

2012 JINST 7 C01083

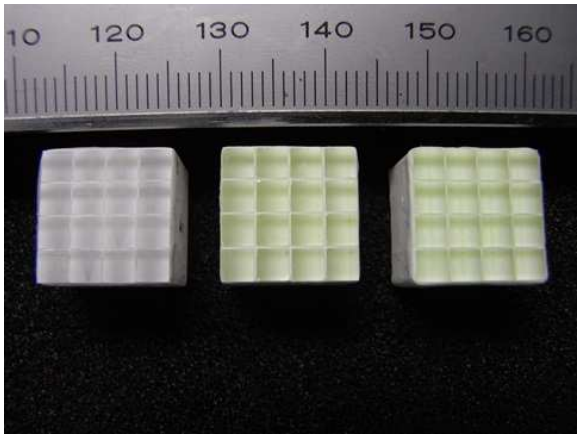

Figure 3. A picture of the scintillator matrices used with the MPPC array. (From left to right: Ce:LYSO, Pr:LuAG, Pr:LuAG(WLS)). The gaps between each element are filled by $BaSO_4$ as a reflector.

to 420 nm light. These scintillator matrices were fabricated to have geometries precisely matching the MPPC array, namely, a 4×4 array of $3\times3\times10\,\mathrm{mm}^3$ pixels, and a 0.2 mm gap between them. Each scintillator pixel is divided with a reflective $BaSO_4$ layer of 0.2 mm thickness. Figure 3 shows a picture of the 4×4 matrices consisting of Ce:LYSO(right), Pr:LuAG(center) and Pr:LuAG(WLS) (right). The optical grease was used between the scintillator matrices and the surface of the MPPC array as well.

The performance of the MPPC array coupled with these pixelized scintillators was evaluated by the energy spectra of a ^{137}Cs source. Here we corrected non-linear response to incident gamma-ray energy, since the MPPCs has limited counting efficiency to large number of photons as described in section 1. As discussed in detail in literature (e.g., [15]), the relation is well represented by a simple function of the form $\mathrm{ADC(ch)} = a[1-\exp(-bE(\mathrm{keV})/a)]$, where ADC (ch) is a measured channel of the CSADC, E (keV) is the energy of gamma rays, and a,b are fitting constants. This calibration was conducted using several kinds of gamma-ray source and the parameters were also decided; covering 59.5 to 1275 keV by ^{241}Am, ^{57}Co, ^{133}Ba, ^{22}Na, and ^{137}Cs sources. Eventually we obtained energy spectra of ^{137}Cs source for all channels for each scintillator matrices. The average values of energy resolutions for the 662 keV photoelectric peak measured with Ce:LYSO, Pr:LuAG, and Pr:LuAG (WLS) matrices were 13.8%, 14.7%, and 14.0%(FWHM), respectively, where the energy resolution variations among the 16 pixels were $\pm12.5\%$, $\pm4.8\%$, and $\pm8.4\%$, respectively. Finally a direct comparison of output charges from the MPPC array was made for different scintillators. It was clear that the output charge from the MPPC array with the Pr:LuAG(WLS) matrix was about 30% larger than that of the Pr:LuAG matrix as expected.

4 Charge division readout

When our detectors are integrated as a complete PET scanner, the large number of channels is likely to be problematic. Since larger readout electronics are required, along with the number of detector channels, costs, power consumption and equipment size would all diverge. In response, a resistor network technique is well established, especially for multi-anode PMTs having several

2012 JINST 7 C01083

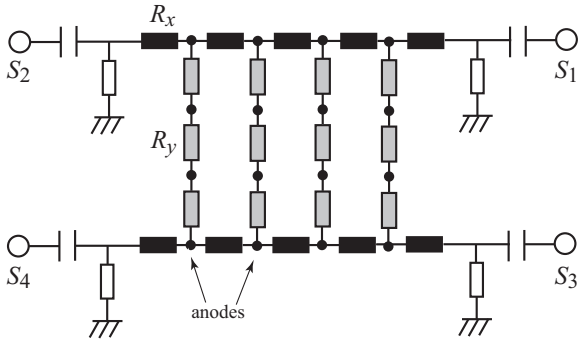

Figure 4. A schematic diagram of the resistor network. The black circles represent the positions of the MPPC array anodes. Boxes filled with black and gray show the arrangement of the resistor groups R_x and R_y (see also the text). The four readout points are indicated by $S_i (i = 1,2,3,4)$.

tens of anodes. A similar method was applied for the MPPC array, configuration of which is shown in figure 4. In this paper, we used a ladder-like network where we defined the grouping of resistors in x and y directions as R_x and R_y, respectively. There is a huge degree of freedom in the ohmic values of individual resistors and means of connection, hence we conducted optimizations of the resistor values from the perspective of positional resolution, as discussed later in this section. Here, we applied 51 and 100 Ω for R_x and R_y, respectively. We first present a successfully reconstructed flood image in figure 5 (top), which was produced as follows. The ^{137}Cs source was exposed to the detector at 0°C consisting of the LYSO scintillator matrix and the MPPC array with a bias voltage of 71.9 V as well as the other measurements reported in this paper. We have four readout channels for these 16 anodes. Each signal is led to the linear fan-in fan-out module and separated into two lines. One is connected to the CSADC and the other is summed over four lines to generate a trigger with the discriminator. The x and y positions of interaction are calculated by the following equations of $x = (S_1 - S_2 + S_3 - S_4)/(S_1 + S_2 + S_3 + S_4)$ and $y = (S_1 + S_2 - S_3 - S_4)/(S_1 + S_2 + S_3 + S_4)$, where S_i is the recorded charge from the channel as indicated in figure 4. Subsequently we obtain the flood image (figure 5 (top)) where all the pixels are nicely resolved. Although the outer pixels tend to be broader peaks, no confusion is recognized. We also extract the projections of the bottom row and the left column in figure 5 (bottom). Subsequently the reconstructed position is calibrated to match the real detector dimension, whereupon a positional resolution is evaluated. We fit the Gaussian to each peak in one dimensional profiles like figure 5 (bottom) and then obtained the averaged FWHM in both x and y directions (σ_x and σ_y) as 0.27 and 0.26 mm, respectively. We could also extract energy spectra from all pixels by selecting events around the corresponding peak in the flood image. Figure 6 presents the ^{137}Cs gamma-ray spectra after the linearity correction described in section 3. The averaged energy resolution is 9.9% (FWHM) with this register network readout, which is better than with the discrete readout system used in section 3. This is probably because the resistor chain readout could collect the charges triggered, even by leaking scintillation photons to neighboring pixels. The greater the charges involved, naturally, the better the energy resolution.

As mentioned above, there are too many degrees of freedom in the resistor parameters. We tried just 3 criteria with R_x and R_y to minimize the averaged position resolution, $\sigma_r = \sqrt{\sigma_x^2 + \sigma_y^2}$. First we changed $R_x = R_y$, the result of which is shown in figure 7 (left). The larger ohmic value

2012 JINST 7 C01083

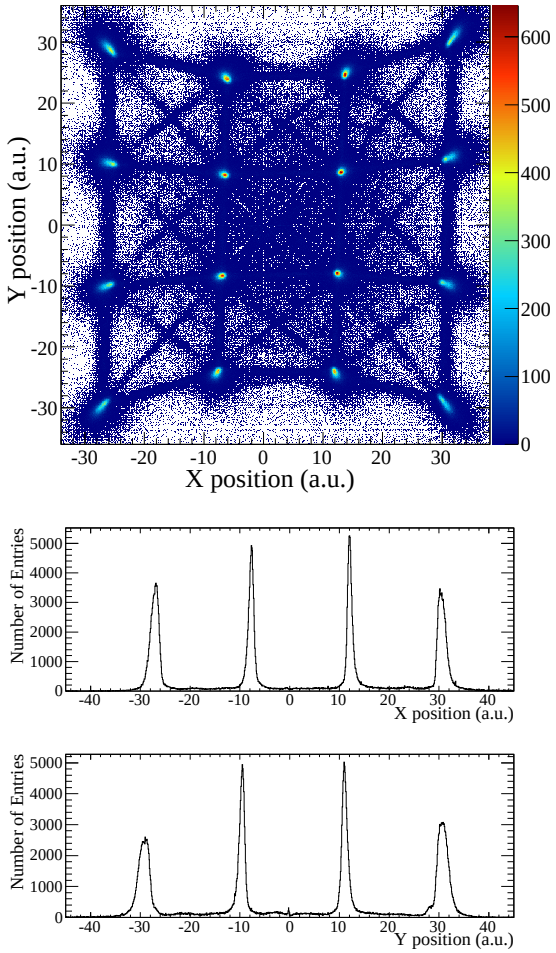

Figure 5. (Top) The flood field image of a ^{137}Cs source irradiation without energy cuts. (Middle) A count profile in the X-direction from the bottom row in the flood image. (Bottom) The same as above but in the Y-direction from the left column in the flood image.

seems preferable. Second we fixed $R_x = 39\ \Omega$ and searched for the best R_y as presented in figure 7 (middle). In this plot $R_y = 82\ \Omega$ was the best, despite possible fluctuation. This result may indicate the optimal combination of R_x and R_y as $Rx/Ry \sim 1/2$. Finally we scanned R_x with the R_x/R_y ratio fixed at 1/2 as shown in figure 7 (right). We confirmed that $(R_x, R_y) = (51\ \Omega, 100\ \Omega)$ was optimal among the data sets we had, though better solutions may also exist.

5 Waveform acquisition

A number of dark counts is an outstanding problem for a scintillation detector utilizing MPPCs as discussed. Waveform sampling in the GHz range will not only enable us to eliminate the contamination of the dark counts but also enable pulse shape discrimination, which is applicable for depth-of-interaction PET detectors with fast scintillators e.g., [16, 17]. Although conventional devices such as flash ADCs have been capable of realizing fast waveform digitizers, the rising cost

2012 JINST 7 C01083

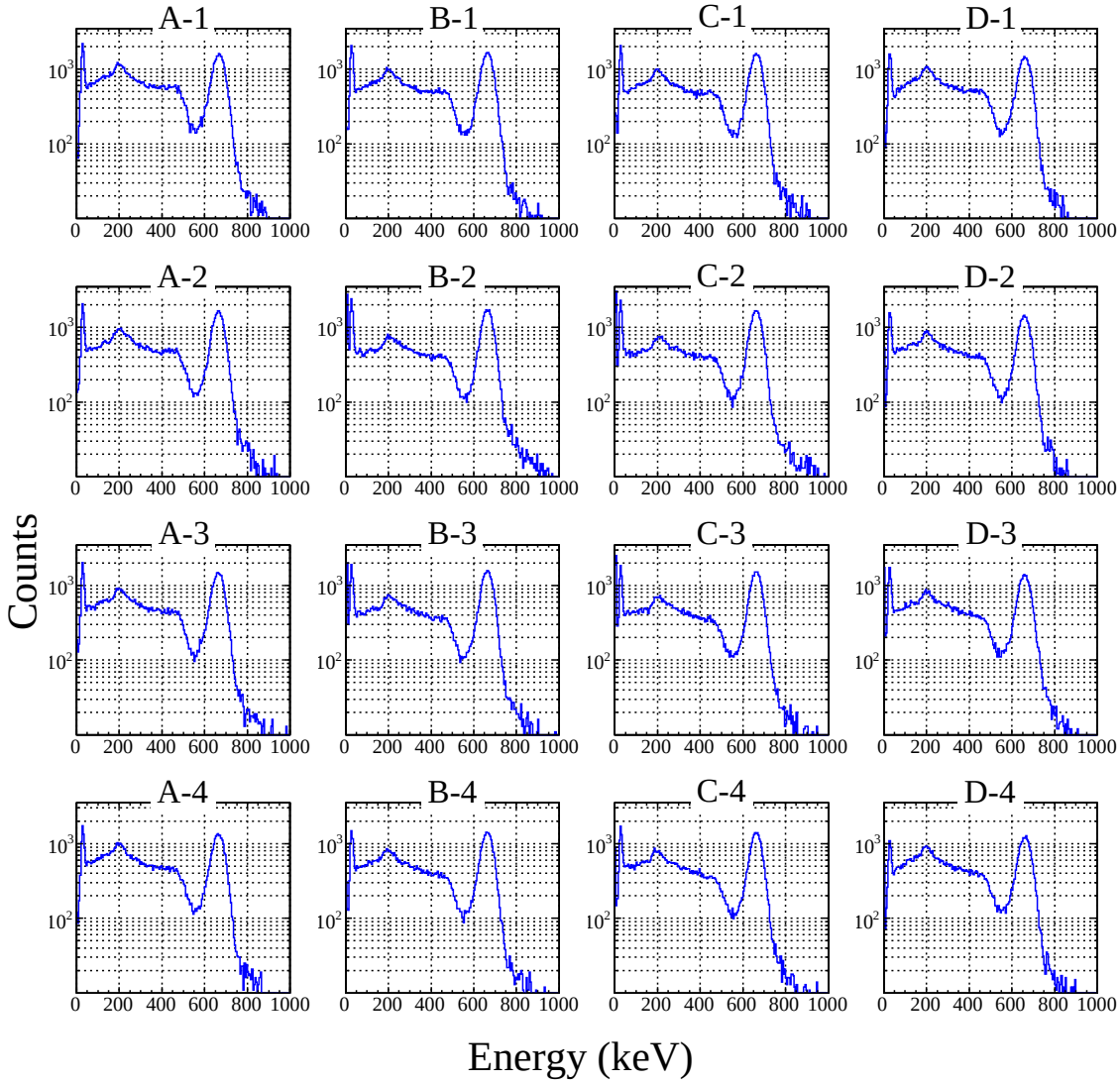

Figure 6. Energy spectra of the ^{137}Cs source, reconstructed from the flood image.

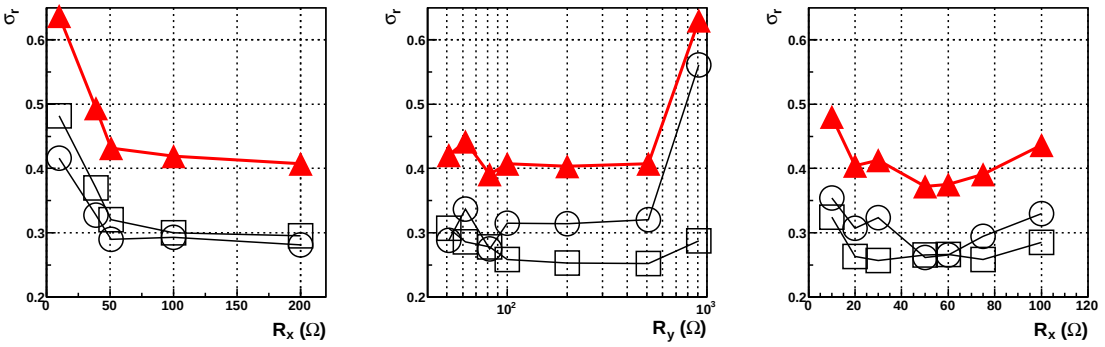

Figure 7. The averaged position resolutions with various resistances. (Left) The case of $R_x = R_y$. (Middle) $R_x = 39\ \Omega$. (Right) $R_x : R_y = 1 : 2$. See text for details.

2012 JINST 7 C01083

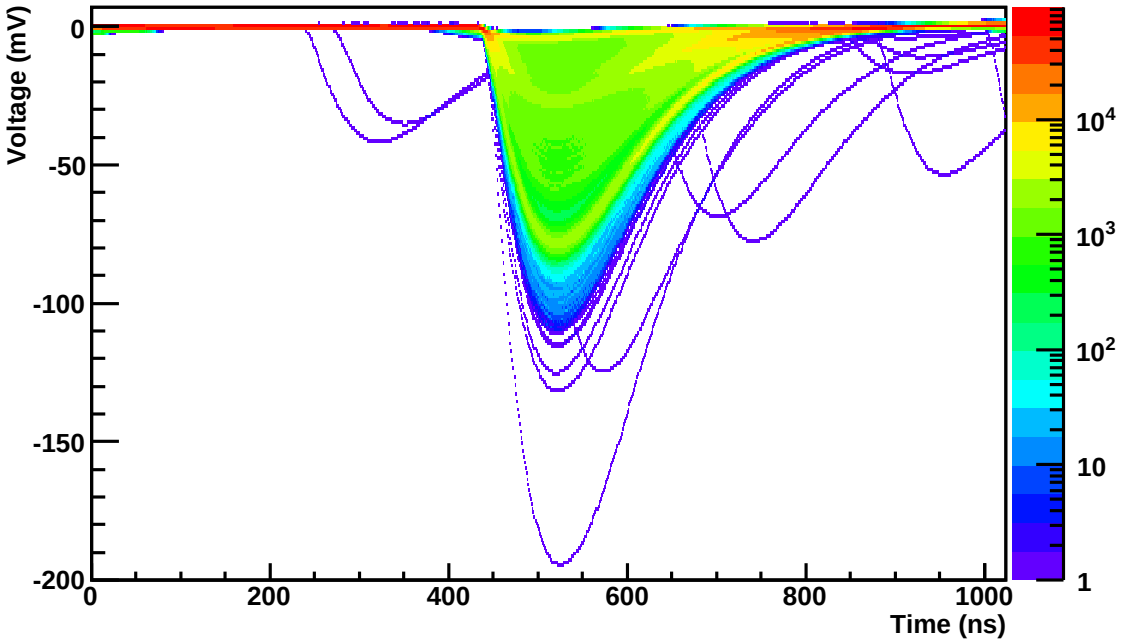

Figure 8. Stacked waveforms after the digital filtering described in the text. The ^{137}Cs source is irradiated to the LYSO crystal.

and power consumption is inevitably a major concern for units involving high channel densities like PET scanners. As a solution, a switched capacitor array chip is alternatively becoming a popular device. The Domino Ring Sampler 4 (DRS4) [18] is one such analog ASIC, which is designed for flexible usage in wide-ranging experimental fields. DRS4 implements 8+1 channels operational up to 6 Gsamples/s and at quite low power consumption. We employed the DRS4 evaluation board [18] and operated at a sampling rate of 1 GHz. Aiming to determine the potential of this approach, here we used a 50 μm type single channel MPPC of 3×3 mm^2 in combination with a LYSO crystal of $3\times3\times10$ mm^3. The MPPC is operated at a gain of 7.5×10^5 at 20°C, whereupon the signal is fed into a fast current amplifier (Philippes 6954) and then simply divided by a linear fan-in/fan-out module. One of the analog signals is connected to the DRS4 board and the other is discriminated to generate a trigger to the DRS4.

To improve the energy resolution and effective energy threshold, we applied a recursive digital filter to improve the signal-to-noise ratio as follows. Using Fast Fourier Transformation, we first produced frequency spectra from waveforms obtained in cases with and without the ^{137}Cs source where we found the gamma-ray triggered signals occupied the frequency space of $<$100 MHz. The digital filter is described as $y[i] = \alpha y[i-1] + (1-\alpha)x[i]$, where $x[i]$ and $y[i]$ are the raw and filtered pulse heights for the i-th data point, and α is a parameter. This filter works as a low-pass filter so that we decided that α had a cutoff frequency of 100 MHz. Eventually we obtained the waveform processed by this filter as presented in figure 8, in which we also see several intrinsic β-decay signals derived from the radio-isotopes of Lu contained in the LYSO crystal. We could extract the pulse height spectrum from this data, as shown in figure 9, which demonstrates the spectroscopic capability as low as we can fully recognize the 32 keV line.

2012 JINST 7 C01083

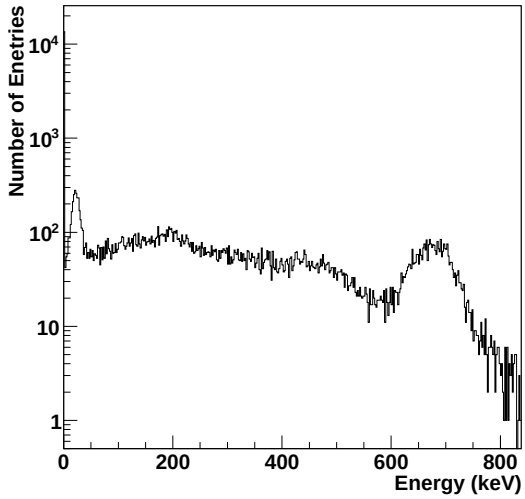

Figure 9. Pulse height spectrum of ^{137}Cs extracted from the filtered waveforms.

When we use the CSADC, we set the gate width as long as the maximum pulses sufficiently enclosed. However this width is too long for pulses triggered by gamma-rays with less energy. Now that we have the waveform information, we could integrate signals over a certain time window like the CSADC, dynamically varying the integration width along with pulse heights. Starting with the digital filtered waveform, we integrated the signal voltages during the pulse over a threshold which we defined as twice as high as the background level deviations. We performed a direct comparison of charge spectra calculated with the fixed gate (like the CSADC) and the dynamic gate width, using a ^{109}Cd source. The result is presented in figure 10, where the 22 keV peak is clearly identified with the variable gate method. The waveform acquisition and detailed analysis has been successfully proved as a powerful method for noise reduction. We note that in this analysis the fixed gate width is optimized for 88 keV peak events hence no significant improvement in energy resolution is recognized in figure 10. We think a more apparent difference will appear when we measure a wider energy range, for instance, with ^{22}Na and ^{109}Cd sources simultaneously.

6 Discussion and conclusion

In this paper, we first presented the excellent timing performance of the MPPCs in comparison to the APDs. The results of our experiment clearly show that MPPCs have promising applicability for ToF-PET scanners. A commercially available ToF-PET scanner (Phillips) recently achieved $\sim$ 500 ps, which is slightly better than our presented result. However, we have already achieved comparable or better timing performance using recent products of MPPC arrays [19] and a dedicated LSI [20] in the laboratory.

We also described the performance of a large-area monolithic MPPC array newly developed by Hamamatsu Photonics K.K. for PET applications. This array consists of 4×4 MPPCs of 3×3 mm^2 pixels, with excellent uniformity of $\pm7.2\%$ in gain variations over the pixels. We tested the performance of the gamma-ray detector with the MPPC array and three scintillator matrices. Based

2012 JINST 7 C01083

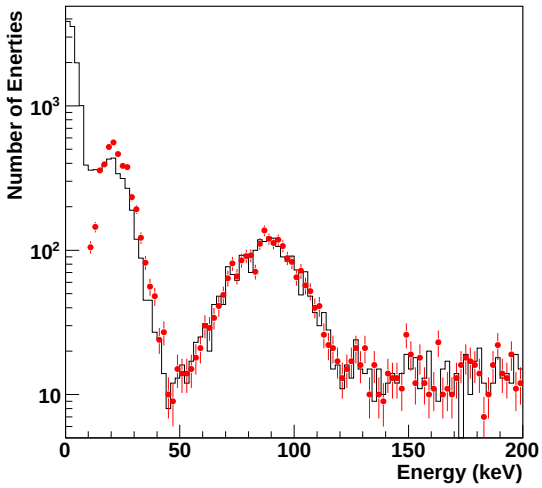

Figure 10. Comparison of ^{109}Cd spectra between the two methods. The solid histogram is obtained by signal integration over the fixed time width, jsut as for the CSADC measurement. The plot with errors presents integration with dynamic widths for the digital-filtered waveforms, in which the 22 keV peak obviously appeared.

on the discrete readout system, the averaged FWHM energy resolutions for 662 keV gamma rays were 13.8, 14.7 and 14.0%, for Ce:LYSO, Pr:LuAG and Pr:LuAG(WLS) matrices, respectively. Although the Ce:LYSO matrix was the best due to the appropriate emission wavelength for the MPPC, we preferred Pr:LuAG from the perspective of the better timing resolution for ToF-PET applications. Improving the quantum efficiency of MPPCs to around 300 nm is highly expected. We also applied the resistor network readout system whereby all pixels were nicely resolved with a typical position resolution of 0.3 mm. The energy resolution was an average of 9.9% at 662 keV. These results indicate the monolithic MPPC array could be useful for medical imaging sensors. Targeting applications such as DoI-PET, we presented the power of the waveform acquisition system for the MPPC. Although a PET scanner uses only limited energy ranges around 511 keV, in several cases, the signal intensity could be much smaller than that presented in this paper. For example, Yamamoto et al. (2010) [17] demonstrate the DoI-PET/MRI detector with the waveform acquisition, based on the differences in the decay time constants of the sensor head scintillators. The system employs optical fibers between the scintillator inside the MRI instruments and the MAPMT outside, where the light intensities are suppressed by a factor of ~ 10. In such cases, a lower energy threshold is required in the application. We demonstrated the noise reduction power with a single MPPC element in combination with the Ce:LYSO, by the clear detection of the 22 keV peak using the DRS4 evaluation board. Further studies are expected for a sophisticated signal processing system, which could also be applicable to other field experiments.

Acknowledgments

This work was supported by Grant-in-Aid for Scientific Research(S), KAKENHI 22220010.

2012 JINST 7 C01083

References

[1] W.W. Moses, *Trends in PET imaging*, *Nucl. Instrum. Meth.* **A 471** (2001) 209.

[2] J. Malamitsi et al., *Preliminary results on the role of PET/CT in initial staging, restaging, and management of lung cancer*, *Nucl. Instrum. Meth.* **A 569** (2006) 319.

[3] H. Peng et al., *Proof-of-principle study of a small animal PET/field-cycled MRI combined system using conventional PMT technology*, *Nucl. Instrum. Meth.* **A 612** (2010) 412.

[4] C. Woody et al., *Preliminary studies of a simultaneous PET/MRI scanner based on the RatCAP small animal tomography*, *Nucl. Instrum. Meth.* **A 571** (2007) 102.

[5] J. Kataoka et al., *Development of an APD-Based PET Module and Preliminary Resolution Performance of an Experimental Prototype Gantry*, *IEEE Trans. Nucl. Sci.* **NS-57** (2010) 2448.

[6] K. Yamamoto et al., *Development of Multi-Pixel Photon Counter (MPPC)*, *IEEE Trans. Nucl. Sci. Conf. R.* **N30-102** (2006) 1094.

[7] K. Yamamoto et al., *Development of Multi-Pixel Photon Counter (MPPC)*, *IEEE Trans. Nucl. Sci. Conf. R.* **N24-292** (2007) 1511.

[8] A. Nassalski et al., *Multi Pixel Photon Counters (MPPC) as an Alternative to APD in PET Applications*, *IEEE Trans. Nucl. Sci.* **NS-57** (2010) 1008.

[9] H. Alva-Sánchez et al., *Initial characterization of a benchtop microPET system based on LYSO crystal arrays and Hamamatsu H8500 PS-PMTs*, *Nucl. Instrum. Meth.* **A 604** (2009) 335.

[10] M. Conti et al., *Comparison of Fast Scintillators With TOF PET Potential*, *IEEE Trans. Nucl. Sci.* **NS-56** (2009) 926.

[11] K. Kamada et al., *Scintillation Properties of 2-Inch-Diameter Pr:$Lu_3Al_5O_{12}$ (LuAG) Single Crystal*, *IEEE Trans. Nucl. Sci.* **NS-56** (2009) 570.

[12] M. Yoshino et al., *The development and performance of UV-enhanced APD-arrays for high resolution PET imaging coupled with pixelized Pr:LuAG crystal*, *Nucl. Instrum. Meth.* **A 643** (2011) 57.

[13] T. Kato et al., *Development of a large-area monolithic 4×4 MPPC array for a future PET scanner employing pixelized Cs:LYSO and Pr:LuAG crystals*, *Nucl. Instrum. Meth.* **A 638** (2011) 83.

[14] C.I. Kim et al., *Time-of-flight PET detector based on multi-pixel photon counter*, *IEEE Trans. Nucl. Sci. Conf. R.* **M95-73** (2009) 2636.

[15] M. Szawlowski et al., *Spectroscopy and timing with Multi-Pixel Photon Counters (MPPC) and LYSO scintillators*, *IEEE Trans. Nucl. Sci. Conf. R.*, **NM1-5** (2007) 4591.

[16] N. Inadama et al., *Performance evaluation for 120 four-layer DOI block detectors of the jPET-D4*, *Radiol. Phys. Technol.* **1** (2008) 75.

[17] S. Yamamoto et al., *Design and performance from an integrated PET/MRI system for small animals*, *Ann. Nucl. Med.* **24** (2010) 89.

[18] S. Ritt et al., *Application of the DRS chip for fast waveform digitizing*, *Nucl. Instrum. Meth.* **A 623** (2010) 486.

[19] T. Kato et al., *A novel gamma-ray detector with sub-millimeter resolutions using a monolithic MPPC array with pixelized Ce:LYSO and Ce:GGAG scintillators*, to appear in proceedings of *8th Hiroshima Symposium (Taipei)* (2012).

[20] H. Matsuda et al., *Development of an ultra-fast ASIC for future PET scanners using TOF-capable MPPC detectors*, to appear in proceedings of *8th Hiroshima Symposium (Taipei)* (2012).

2012 JINST 7 C01083